# Mossbauer spectroscopic and computational investigation of an iron cyclopentadienone complex

Ikram Yagoub, Martin Clémancey, Pierre-Alain Bayle, Adrien Quintard, Guillaume Delattre, Geneviève Blondin, Amélie Kochem

# Mössbauer spectroscopic and computational investigation of an iron cyclopentadienone complex.

*Ikram Yagoub,[†] Martin Clémancey,[†] Pierre-Alain Bayle,[&] Adrien Quintard,[¶] Guillaume Delattre,[†] Geneviève Blondin, [†] * and Amélie Kochem[†] **

† Univ. Grenoble Alpes, CNRS, CEA, LCBM (UMR 5249), F-38000 Grenoble, France.

& Univ. Grenoble Alpes, CEA, INAC, MEM, F-38000 Grenoble, France.

¶ Aix Marseille Univ, CNRS, Centrale Marseille Ism2, Marseille, France.

(cyclopentadienone)iron carbonyl complexes • Mössbauer spectroscopy • computational study • chemical activation • iron catalysis.

**ABSTRACT.**

(cyclopentadienone)iron carbonyl complexes have recently received particular attention in their use as catalysts for hydrogenation or transfer hydrogenation reactions including the *N*-alkylation of amines with alcohols. This is due to their easy synthesis from simple and cheap materials, air and water stabilities, and to the crucial metal-ligand cooperation giving rise to unique catalytic properties. Here, we report a Mössbauer spectroscopic and computational investigation of such a complex and of its corresponding activated species prompt for dehydrogenation and hydrogenation reactions. This study affords a deeper understanding on the species formed upon reaction with $Me_3NO$ and on their distribution upon the added amount of oxidant.

**INTRODUCTION.**

The direct catalytic high atom economy and sustainable *N*-alkylation of amine with alcohol through borrowing hydrogen catalysis is considered as one of the most promising methods to access sustainably valuable pharmaceutical ingredients containing amine groups from readily available stable alcohols. For decades, this field has endured dominance of late and mostly noble metal based homogeneous[1] and heterogeneous[2] catalysts. Recently, the development of efficient molecular catalysts based on non-precious, non-toxic and earth abundant metal such as iron encompassed growing interest.[3] Among these catalysts, (cyclopentadienone)iron carbonyl complexes (**[LFe(CO)$_3$]**, further denoted **1**) hold a special place due to their easy synthesis from simple and cheap materials, their air and water stability and to the metal-ligand cooperation giving rise to unique catalytic properties.[4] The proposed mechanism proceeds as following: the pre-catalyst **1** is thermally, photochemically and/or chemically activated via CO decoordination (Scheme 1). It is proposed to lead to the formation of the corresponding complex **[LFe(CO)$_2$]**

that is prompt to dehydrogenate the alcohol forming an activated carbonyl intermediate.[5] The resulting dihydrogen is temporarily stored on the molecular catalyst. A subsequent condensation with the amine forms an imine, which then undergoes hydrogen transfer by the complex **[(HL)FeH(CO)$_2$]** (further denoted **2**) to give the *N*-alkylated product with regeneration of the active iron complex. The overall process is hydrogen and redox neutral and produces water as the only stoichiometric by-product. Consequently, this catalytic domino process allows considerable step, waste and atom economies compared to traditional sequential reactions. As such, it offers a ground-breaking eco-compatible methodology for C-N bond formation. Another advantage of these catalysts lies in the fact that the use of a strong external base such as KO$^t$Bu is not required to obtain an efficient catalytic system compared to what is done with numerous pincer type complexes for instance. As such, they are considered as base free catalytic systems. Note that it does not exclude the possibility of the amine substrate to act possibly as a base. The first iron-cyclopentadienone catalyzed *N*-alkylation of amine with alcohol was reported in 2014 by Barta and collaborators[5] followed by numerous other examples.[6–8 and references therein]

**Scheme 1.** *N*-alkylation of amine with alcohol catalyzed by (cyclopentadienone)iron carbonyl complex.

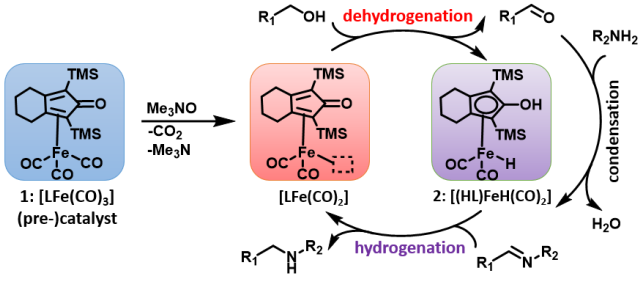


Given this reactivity, (cyclopentadienone)iron carbonyl complexes are able to catalyze diverse reactions including the hydrogenation or transfer hydrogenation of carbonyl and imine

compounds, the direct amination of carbonyl compounds and the hydrogenolysis of esters to alcohols to name a few.[4,6–8] Usually, an outer-sphere mechanism is proposed for these hydrogenation reactions with two key intermediates named **[LFe(CO)$_2$]** and **2** as for the *N*-alkylation of amines. It may be noticed that conversely to **2** that has been isolated and characterized, **[LFe(CO)$_2$]** has never been isolated and no spectroscopic signatures have been reported so far.

Among the different activation modes to generate **[LFe(CO)$_2$]** active for dehydrogenation reactions, the convenient use of a chemical activator such as $Me_3NO$ accounts for the most employed methodology in the literature.[6–8 and references therein] In principle, one equivalent of trimethylamine-*N*-oxide is sufficient to convert stoichiometrically **1** into **[LFe(CO)$_2$]**. However, varying amounts of $Me_3NO$ from one up to several equivalents are used to activate the precatalyst. We anticipate that the ratio pre-catalyst/$Me_3NO$ may influence the distribution and the type of species formed upon activation of the precatalyst. Herein we report a Mössbauer spectroscopic investigation of the precatalyst **1** and its corresponding active species, in combination with quantum chemistry. We address the effect of the quantity of $Me_3NO$ used in respect to **1** on the distribution of the iron species formed during the course of CO decoordination. We will show here that spectroscopic and computational studies support the formation of trimethylamine containing complexes. This questions the adage considering the (cyclopentadienone)iron carbonyl as a base free catalytic system.

## EXPERIMENTAL SECTION

**General.** All manipulations were performed under an atmosphere of purified argon using standard Schlenk and glove-box techniques. Anhydrous toluene (Sigma Aldrich, ACS reagent)

was used as received. $CDCl_3$ (Eurisotop) was pass through a short pad of neutral alumina prior to use. **[FeL(CO)$_3$]**[9,10] and **[(HL)FeH(CO)$_3$]**[11] were prepared according to published procedures.

**Instrumentation.** $^1$H and $^{13}$C-NMR spectra were recorded at 400 MHz on a Varian Avance III 400 spectrometer. UV-visible spectra were obtained with a Hewlett Packard HP 89090A spectrometer. Mössbauer spectra were recorded on powder samples or on toluene solutions contained in Delrin cups of natural-abundance $^{57}$Fe compounds (iron complexes at 22mM). Mössbauer spectra were recorded at 80 K on a low-field Mössbauer spectrometer equipped with a Janis SVT 400 cryostat or on a strong-field Mössbauer spectrometer equipped with an Oxford Instruments Spectromag 4000 cryostat containing a 8 T split-pair superconducting magnet. The spectrometer was operated in a constant acceleration mode in transmission geometry. All velocity scales and isomer shifts are referred to the metallic iron standard at room temperature. Analysis of the data was performed with a homemade program.[12,13] Full experimental details including samples preparation, spectroscopic ($^1$H and $^{13}$C NMR, Mössbauer) and details of computational calculations are given in the Supporting Information.

**Computational Details.** Geometry optimizations and Mössbauer parameters calculations were carried out using the ORCA program, version 3.0.3.[14] Geometry optimizations of all compounds were performed at the TPSSh[15] level of theory (employing the RIJCOSX approximation[16,17]), including the ZORA scalar relativistic method[18,19], relativistically recontracted versions of the Karlsruhe def2-TZVP basis sets[20,21] and D3-dispersion correction.[22,23] Solvation effects were accounted for using the Conductor-like Screening Model (COSMO).[24] Geometry optimization was followed by a frequency calculation to obtain the Gibbs energy (taken as the sum of electronic and thermal free energies). Single-point calculations were performed using the hybrid GGA functional B3LYP (20% HF exchange) to obtain electron-density values at the Fe nuclear

positions that were used to derive the isomer shifts. A mixed basis set was used that consists of the core-polarized CP(PPP) basis set[25,26] on Fe atoms and DKH-def2-TZVP[20,21] on all other atoms. Scalar relativistic effects in the Mössbauer isomer shift calculations were accounted for using the second-order Douglas−Kroll−Hess approximation. The $^{57}$Fe Mössbauer isomer shifts were calibrated using the extended ("whole") calibration parameters according to Neese,[27] which includes previously reported[28,29] calibration sets. $\delta_{iso}=\alpha(\rho_0-C)+\beta$, with: $\alpha$ = -0.173830492, $\beta$ = 0.37718458 and C = 23615. $^{13}$C NMR chemical shift values were computed using the gauge-independent atomic orbital (GIAO) method incorporated[30,31] into Orca 4.21,[32] the B3LYP functional, and the relativistically recontracted versions of the Karlsruhe def2-TZVP basis sets[20,21] were used. Isotropic shielding values obtained from the computation were referenced to the carbon isotropic shielding values of tetramethylsilane (TMS) computed at the same level of theory.

**RESULTS**

*Mössbauer spectroscopy.* Most of the *N*-alkylation of amine with alcohol reactions involving **1** and **2** have been performed in toluene.[6–8 and references therein] $^{57}$Fe-Mössbauer spectroscopy is sensitive to the electron density on the iron site, and therefore to changes in the coordination sphere. This prompted us to investigate the frozen toluene solutions of these complexes by Mössbauer spectroscopy. Because the concentration can be as high as 50 mM, no enrichment in $^{57}$Fe was required. Both complexes were synthetized according to previously published procedures.[9–11] Spectra *a* and *b* in Figure 1 correspond to the 80 K and zero-field spectra of **2** and **1**, respectively. Both species are characterized by a doublet. The Mössbauer parameters are listed in Table 1. The isomer shift for the hydride complex **2** is slightly smaller than that of the tricarbonyl species **1** (0.02 and 0.06 mm $s^{-1}$, respectively) whereas the reverse order is

determined for the quadrupole splitting values (1.72 and 1.49 mm $s^{-1}$, respectively). The Mössbauer nuclear parameters for **1** in frozen solution are similar to those determined at 80 K on a powder sample ($\delta$ = 0.06 mm $s^{-1}$ and $\Delta E_Q$ = 1.47 mm $s^{-1}$, see Figure S1), indicating that the structure is retained upon dissolution in toluene. Measurements at 5 K on both the solid and the toluene solution demonstrate the diamagnetic character of **1** (see Figure S1 and Table S1).

We then turned to the investigation of the mode of action of trimethylamine-*N*-oxide on **1**. Three different solutions were studied, generated by adding 1, 2 and 4 equivalents of $Me_3NO$ at room temperature. UV-visible monitoring evidenced completion of the reactions after 10 minutes (see Figure S2). Mössbauer spectra of the corresponding frozen solutions are reproduced in Figure 1 (see spectra *c*-*e*). The comparison with spectrum *b* clearly evidenced that the starting complex is still present in solutions with 1 and 2 equiv of $Me_3NO$. A second iron site characterized by a doublet with lines at ≈–0.35 and ≈+0.75 mm $s^{-1}$, is identified in spectrum *c* that became the major component in spectrum *d*. A perusal of this series of four spectra also allows to evidence a third doublet with the low and high velocity lines located at ≈0.0 and ≈1.1 mm $s^{-1}$, respectively. Accordingly, spectra *c*-*e* were simultaneously simulated considering three doublets, one being that of **1** previously determined from spectrum *b*, the other two being labeled **3** and **4**. The result is shown in Figure 1 as bold solid lines overlaid on the experimental spectra. Parameters are listed in Table 1.

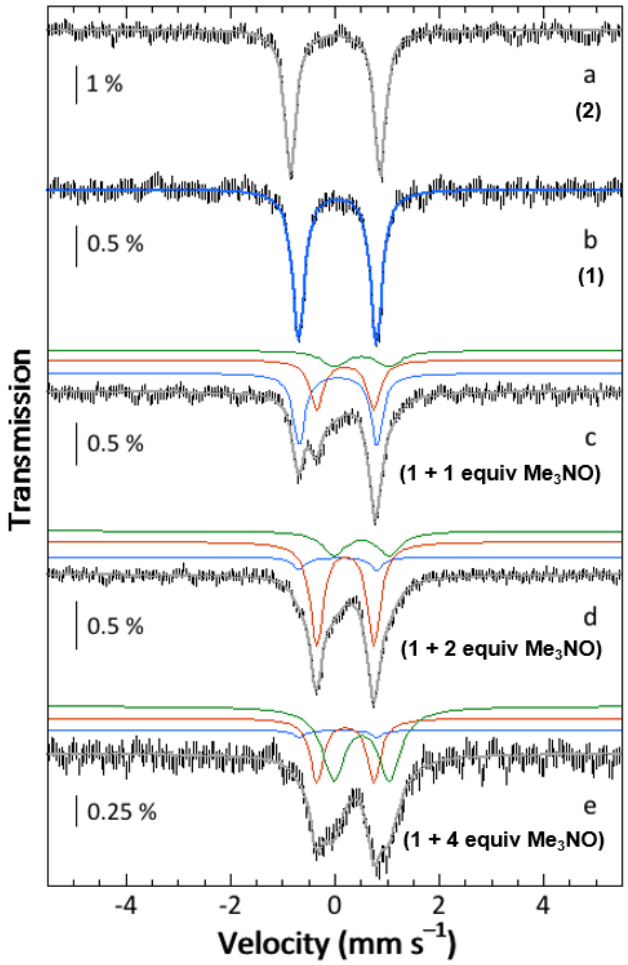


**Figure 1.** 80 K and zero-field Mössbauer spectra (hatched bars) of frozen toluene solutions of **2** (*a*), **1** (*b*), **1** + *n* equiv $Me_3NO$ (*n*=1 (*c*); *n*=2 (*d*); *n*=4 (*e*)). Spectrum *a* was corrected from the contribution (12 %) of an impurity ($\delta$ = 0.26 mm $s^{-1}$, $\Delta E_Q$ = 1.87 mm $s^{-1}$). Simulations are shown as grey solid lines, except for spectrum *b*. Deconvolution is shown above spectra *c*-*e* with the color code: **1** in blue; **3** in red; **4** in green. See Table 1 for parameters.

**Table 1**. Mössbauer parameters determined from simulations of spectra *a*-*e*. Only the absolute value of the quadrupole splitting can be experimentally determined from zero-field Mösbauer spectra. Uncertainties are ± 0.02 mm $s^{-1}$, ±0.05 mm $s^{-1}$, ±0.02 mm $s^{-1}$, and ±5 % on $\delta$, $\Delta E_Q$, $\Gamma_{fwhm}$

and contribution, respectively. Values in parenthesis correspond to those determined by DFT calculations.

| Solution | **2** | **1** + *n* $Me_3NO$ | | | |
|---|---|---|---|---|---|
| | | *n* | **1** | **3** | **4** |
| $\delta$ (mm $s^{-1}$) | 0.02 (0.04) | | 0.06 (0.06) | 0.20 | 0.51 |
| $\Delta E_Q$ (mm $s^{-1}$) | 1.72 (1.92) | | 1.49 (1.49)[a] | 1.09 | 1.06 |
| $\Gamma$ (mm $s^{-1}$)[b] | 0.25 | | 0.28/0.27 | 0.31 | 0.54 |
| Contribution (%) | 100 | 0 | 100 | 0 | 0 |
| | | 1 | 45 | 34 | 18 |
| | | 2 | 8 | 71 | 28 |
| | | 4 | 3 | 32 | 62 |

[a] The close to 1 value determined for the η parameter (0.97, see SI) indicates that the sign of $\Delta E_Q$ is not relevant.

The linewidth for species **4** is significantly larger than that for **3**, suggesting a mixture of closely related structures for **4**, in contrast to a better-defined environment for the Fe site in **3**. The isomer shifts of species **3** and **4** generated upon action of $Me_3NO$ are significantly larger than that of **1**, indicating successive and similar changes in the coordination sphere of the iron site. As anticipated, the starting complex **1** remains the major species (45 %) upon the addition of 1 equiv of $Me_3NO$ whereas a drastic decrease to 8 % is observed upon reaction with 2 equiv. Only traces of **1** (3 %) are detected after the addition of 4. equiv. This Mössbauer study evidenced that more than one equivalent of $Me_3NO$ are required for **3** to become the major species (34 % in spectrum *c*, 71 % in spectrum *d*) and that the addition of more than 2 equiv is detrimental (32 % in spectrum *e*). Concomitantly, **4** continuously increases upon the amount of added oxidant (18, 28, and 62 % in spectra *c*-*e*, respectively). Accordingly, it is tempting to identify species **3** as a key intermediate in dehydrogenation reaction.

*DFT calculations*. In order to provide a clear picture of the electronic structure of **1** and **2**, and to attempt to identify the species formed during the course of the reaction of the pre-catalyst with $Me_3NO$, a computational investigation was carried out using density functional theory (DFT). The calculations of the Mössbauer nuclear parameters closely follow a procedure developed by F. Neese and coworkers.[27,28] Firstly, we focused on the isolated complexes **1** and **2**. Calculated coordination bond distances are over-estimated by 0.05 Å for **1**[9] and 0.03 Å for **2**[11] compared to the X-ray data, as typically observed with current DFT functionals[33] (Figure S3, S4 and Table S2). Isomer shifts and quadrupole splittings derived from DFT calculations are displayed in Table 1. The agreement between experimental and theoretical values is very satisfying with deviations smaller than 0.02 and 0.20 mm $s^{-1}$ for $\delta$ and $\Delta E_Q$, respectively. This comforted us in that calculating Mössbauer parameters will allow identifying the iron coordination spheres in **3** and **4**.

The reaction of the pre-catalyst with $Me_3NO$ was proposed to release volatile $CO_2$ and $Me_3N$ and accordingly form **[LFe(CO)$_2$]**. Early studies showed that the produced $Me_3N$ can remain coordinated to transition-metal carbonyls complexes and that [(diene)Fe(CO)$_2$(NHMe$_2$)] can be produced while using at least two equivalents of $Me_3NO$.[34,35] Thus, we considered the following series of complexes: **[LFe(CO)$_2$]**, **[LFe(CO)$_2$(NMe$_3$)]** and **[LFe(CO)$_2$(NHMe$_2$)]**. For each complex, three conformational isomers were considered depending on the position of the released CO ligand (see Figure 2a and Figures S5-14). The X-ray structure of **1** revealed that one CO ligand is eclipsed with the carbonyl function of L. Hereafter, the $\alpha$-isomer denotes the complex corresponding to the release of this specific CO ligand. The two remaining isomers, denoted $\beta$ and $\gamma$, are anticipated to be very similar. Figure 2b-d gathered the results obtained for

the α- and β-isomers. Those for the γ-isomers, close to those of the β-isomer, are presented in Figure S14.

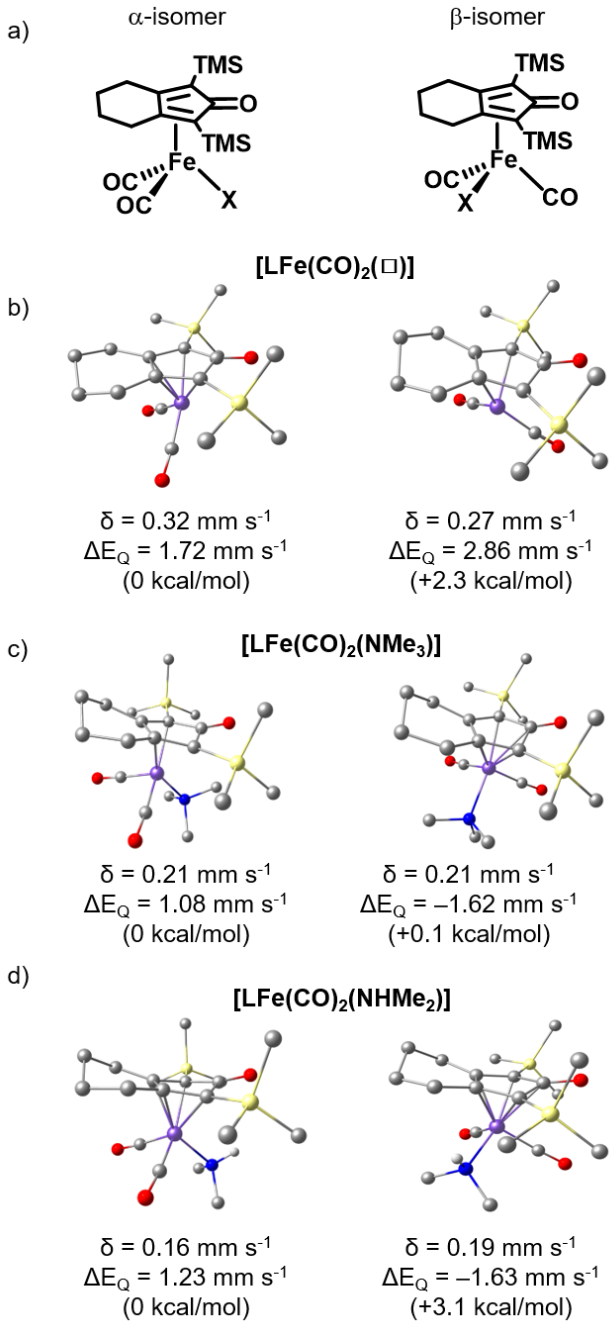


**Figure 2.** (a) Scheme of the α- and β-isomers of **[LFe(CO)$_2$(X)]** (X=vacant, $NMe_3$, $NHMe_2$). (b-d) Geometry optimized structures and corresponding calculated Mössbauer parameters δ and

$\Delta E_Q$. H atoms omitted for clarity except for the secondary amine. Relative energies of the α- and β-isomers in each series of complexes are indicated in brackets.

Whatever the isomer, the removal of one CO, a strong π-acceptor ligand, leads to a significant increase of the isomer shift compared to that of the pre-catalyst (≈0.3 mm $s^{-1}$ for **[LFe(CO)$_2$]** versus 0.06 mm $s^{-1}$ for **1**). As expected, this increase is partially compensated by the coordination of an amine, $NMe_3$ or $NHMe_2$ (≈0.2 mm $s^{-1}$). The isomer shift of **[LFe(CO)$_2$(NHMe$_2$)]** is low compared with that of **[LFe(CO)$_2$(NMe$_3$)]**. This is surprising since the replacement of the trimethylamine by the weaker σ-donor $NHMe_2$ ligand should lead to a higher isomer shift. Deeper analysis of the bond lengths and Mayer bond orders shows that the Fe-N bond is more covalent in the case of **[LFe(CO)$_2$(NHMe$_2$)]** explaining the lower isomer shift (Figure S15). This is attributed to steric hindrance between the protons of $NMe_3$ and the cyclopentadienone ligand that precludes a short Fe-N bond.

Departure of one CO also leads to an increase of the quadrupole splitting ($\Delta E_Q$, absolute values) that is reduced upon coordination of $NMe_3$ or $NHMe_2$. In contrast to the isomer shifts, $\Delta E_Q$ values depend on the isomer. Lower values are determined for the α-isomers than for the β- and γ-forms. However, variations can't be simply related to the variations in the geometry around the iron.

A close examination of Figure 2 reveals that only the parameters of **α-[LFe(CO)$_2$(NMe$_3$)]** closely match those experimentally determined by Mössbauer. Accordingly, we propose species **3** to be the **α-[LFe(CO)$_2$(NMe$_3$)]** complex. Coordination of $NMe_3$ is supported by the characterization of related complexes. Several nitrile complexes **[LFe(CO)$_2$(NCR)]** have been previously isolated and characterized upon reaction of 1.2–1.5 eq of $Me_3NO$ on **1**.[36] Analogously, the complex **[LFe(CO)$_2$(HOCH$_2$Ph)]** was characterized as resulting from the

reaction of **2** with benzaldehyde in toluene.[37] It is also remarkable to notice that the X-ray structures of **[LFe(CO)$_2$(HOCH$_2$Ph)]**[37] and of **[L'Fe(CO)$_2$(PPh$_3$)]** (L' = 2,4-diphenylbiclyclo[3.3.0]octa-1,4-dien-3-one)[38] have revealed a α-conformation, the O and P coordinated atoms being almost in the plane defined by the Fe ion and the L and L' ligand carbonyl function (O–C–Fe–(O/P) torsion angle lower than 3°). A symmetric structure has also been proposed for **[LFe(CO)$_2$(NCCH$_3$)]** from its $^1$H-NMR spectrum.[37] This is in line with calculated energy for the different isomers, evidencing the preferred α-conformation within the series of considered complexes (Figure 2). All together, these observations strongly sustain the generation of **α-[LFe(CO)$_2$(NMe$_3$)]** as the major species upon reaction of $Me_3NO$ with **1**.

Next, we attempted to identify the structures compatible with the Mössbauer parameters determined for species **4** ($\delta$ = 0.51 mm s$^{-1}$ and $\Delta E_Q$ = 1.06 mm s$^{-1}$), keeping in mind that the large linewidth suggests a distribution of the nuclear parameters and thus a distribution for the Fe environment. It may already be noticed that the Mössbauer parameters calculated for **[LFe(CO)$_2$]**, whatever the isomer, are well separated from the desired values, excluding the formation of this complex. Because the reaction of 1 equiv of trimethylamine-*N*-oxide on **1** is not complete, we hypothesized that unreacted $Me_3NO$ may act on the generated complex **3**. Accordingly, we investigated the six different isomers of **[LFe(CO)(NMe$_3$)]** and the three of **[LFe(CO)(NMe$_3$)$_2$]**, the latter resulting from the coordination of an additional trimethylamine in place of the released CO. The departure of two CO ligands from **1** leading to the formation of **[LFe(CO)]** was also considered. Details are presented in the Supporting Information and are summarized below. As it may be anticipated, Mössbauer parameters for **[LFe(CO)]** are larger than those of **[LFe(CO)$_2$]** ($\delta$ > 0.57 mm s$^{-1}$ and $|\Delta E_Q|$ > 2.9 mm s$^{-1}$, see Figure S16). These obtained values are indeed too high to support the formation of **[LFe(CO)]**. Similarly, the

departure of one CO from **[LFe(CO)$_2$(NMe$_3$)]** induced increased isomer shifts for **[LFe(CO)(NMe$_3$)]** ($\delta$ ranging from 0.40 to 0.43 mm s$^{-1}$, see Figure S17), but significantly lower than that determined. Because the corresponding quadrupole splittings are also too large ($|\Delta E_Q|$ ranging from 2.16 to 2.57 mm s$^{-1}$), formation of **[LFe(CO)(NMe$_3$)]** was ruled out. Mössbauer parameters values calculated for **[LFe(CO)(NMe$_3$)$_2$]** are given in Figure 3. Based on the calculated energies, the α-isomer, corresponding to an eclipsed CO ligand with respect to the carbonyl group of L, is disfavored. $\Delta E_Q$ for the β- and γ-isomers are exceeding the desired value by ≈0.5 mm s$^{-1}$ whereas the isomer shifts are perfectly in agreement with the 0.5 mm s$^{-1}$ observed value. It may be noted that former studies have evidenced the exchange of two carbonyl ligands in **1** by two acetonitrile molecules upon photochemical activation of **1** performed in $CH_3CN$, the resulting X-ray characterized **[LFe(CO)(NCMe)$_2$]** complex presenting a β-conformation.[39] We are thus inclined to identify **4** as **β-[LFe(CO)(NMe$_3$)$_2$]**.

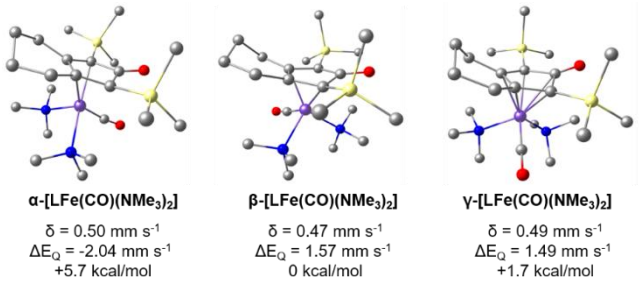


**Figure 3.** Geometry optimized structures of the three conformational isomers for **[LFe(CO)(NMe$_3$)$_2$]**, computed Mössbauer nuclear parameters and relative energy (B3LYP).

*$^{13}$C NMR spectroscopy*. In order to confirm the coordination of $NMe_3$, we then performed an NMR study. The mixture obtained by reacting **[LFe(CO)$_3$]** with two equivalents of $Me_3NO$ contains the species labeled **3** as major and was sufficiently stable on the NMR time scale to be

analyzed . With four equivalents of $Me_3NO$, the fast degradation of the mixture containing mostly the species labeled **4** precludes a similar study.

At magnetic fields above 9.4 T, corresponding to 400 MHz for $^1H$ NMR spectra, the dispersion is not high enough to distinguish in conventional one-dimensional spectra the protons of the precatalyst from the protons of the new species formed. $^{13}C$ NMR shifts extend over a much larger range than proton shifts and are particularly suited to identify diamagnetic iron complexes, even in mixtures. We applied an inverse gated decoupled methodology in which proton decoupling is only applied during the acquisition period. In this case, no polarization transfer from $^1H$ to $^{13}C$ via NOE takes place and therefore, the resulting $^1H$-coupled $^{13}C$ spectrum can be used for quantitative measurements.

Figure 4a shows the proton decoupled $^{13}C$ NMR spectra of **[LFe(CO)$_3$]** taken in $CDCl_3$ solution at 298 K. Integral values for the different $^{13}C$ resonances are identical to the expected values, demonstrating the efficiency of the methodology applied for quantitative measurements (Figure S20). To reduce the acquisition time without weakening the signal-to-noise ratio, a shorter relaxation time was applied (Figure 4a). A 3:6 quantitative ratio is still obtained for the resonance of the coordinated CO ligands and those from the methyl groups of the $SiMe_3$ substituents of L (Figure S21). The same methodology was then applied to measure the $^{13}C$ NMR spectrum of the mixture obtained by reacting **[LFe(CO)$_3$]** with 2 equiv of $Me_3NO$ (Figure 4b). All the characteristic resonances of **[LFe(CO)$_3$]** are observed but the spectrum is clearly dominated by the appearance of a new set of resonances attributed to the formation of a new species. This major species is characterized by the same number of resonances slightly shifted as compared to those of **1**. It is worth noticing the appearance of a new resonance at 58.2 ppm. The resonances at $\delta$ = 214.8 ppm and 0.82 ppm corresponding to the coordinated CO ligands and to

the $SiMe_3$ groups integrate for two and six, respectively, while the resonance at δ = 58.2 ppm integrates for three (Figure S22). This is in agreement with the substitution of one CO by one trimethylamine ligand. The assignment of the resonance at δ = 58.2 ppm to the methyl groups of $Me_3N$ is corroborated by DEPT 135 measurement (Figure S23) and DFT calculations (Figure S19). A ratio of 7.3(±0.5):1 for **[LFe(CO)$_2$(NMe$_3$)]:[LFe(CO)$_3$]** was determined based on the integrals of the $CH_2$ signals (see inset in Figure S22). These results are in line with the Mössbauer data showing that a few percent of unreacted precatalyst remain in solution (see Table 1).

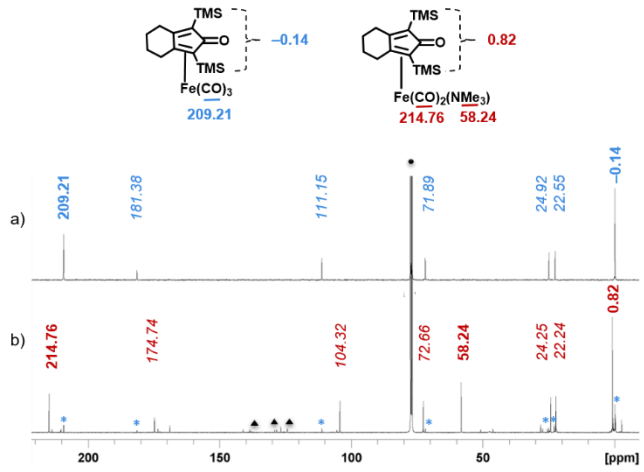


**Figure 4.** Inverse gated proton decoupled $^{13}C$ NMR spectra recorded in $CDCl_3$ of complex **[LFe(CO)$_3$]** a) in absence of $Me_3NO$ and b) reacted with 2 equiv of $Me_3NO$. T = 298 K. Blue starts denote **[LFe(CO)$_3$]** resonances, black triangles and dot denote toluene and chloroform solvent resonances, respectively.

## DISCUSSION

Overall, these experimental and computational studies shed light on the type of species formed during chemical activation of (cyclopentadienone)iron carbonyl complexes and complement

previous studies carried out on photochemical activation. Indeed, it has been previously demonstrated that photocatalytic activation of **[LFe(CO)$_3$]** in acetonitrile at -30 °C gives rise to the formation of stepwise and reversible ligand exchange of all three carbonyl ligands by acetonitrile molecules.[39] In addition, studies conducted with (tetraphenylcyclopentadienone)iron carbonyl complex showed the reversible formation of the corresponding activated species with one vacant coordination site when the photocatalytic activation was performed in toluene in closed vial at room temperature.[40] Despite these studies underlying the role of the solvent and the reaction condition (open or closed vial) on the type of species formed by photochemical activation, too few studies take into account the type of species formed through chemical activation. The most employed methodology in the literature to activate the precatalyst relies on the use of trimethylamine-*N*-oxide as an external oxidant, generating $CO_2$ and $NMe_3$ as byproducts. **[LFe(CO)$_2$]** is often proposed as the activated complex resulting from this chemical activation, despite the coordinating capability of the generated trimethylamine (Figure 5).

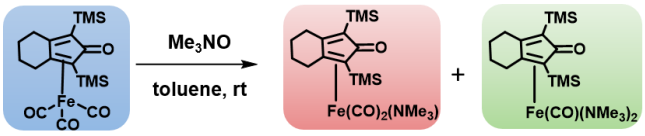


**Figure 5.** Revisited scenario for the chemical activation of (cyclopentadienone)iron carbonyl complex in absence of substrate.

Our studies evidence that the use of $Me_3NO$ leads to complexes with no vacant position, the released CO being replaced by the generated $NMe_3$. We have shown here that the conversion of **[LFe(CO)$_3$]** is never complete when using from one up to four equivalents of $Me_3NO$ at room temperature in toluene. The produced mixtures always contain the precatalyst and two new species in which one or two CO ligands are replaced by trimethylamine were identified. Hence,

under catalytic conditions, we anticipate that the coordination of the alcohol is in competition with that of the generated $NMe_3$. It has been previously evidenced that the X ligand in preformed **[LFe(CO)$_2$(X)]** (X representing phosphine, nitrile or pyridine type ligand) can be substituted by an alcohol.[37] Thus, formation of [LFe(CO)$_2$($NMe_3$)] may not be detrimental for the catalysis but may reduce the catalytic efficiency of the iron complex. Note that heating the solution at 35°C for 20 minutes did not lead to the formation of the 16-electron complex **[LFe(CO)$_2$]**. Generation of $NMe_3$, that is a base, may interfere with the acidic conditions used for the catalysis in some cases. Accordingly, this system cannot be considered as a base-free catalyst. This has been circumvented by the employment of preformed **[(HL)FeH(CO)$_2$]** or **[LFe(CO)$_2$(NCR)]** where only $H_2$ and RCN are liberated, respectively.[41,42] Furthermore, we have shown here that $Me_3NO$ also reacts with [LFe(CO)$_2$($NMe_3$)]. The coexistence of **[LFe(CO)$_2$($NMe_3$)]** and **[LFe(CO)($NMe_3$)$_2$]** irrespectively of the number of $Me_3NO$ equivalents open the door to new questioning regarding the catalytic active species (Figure 5). As such, it demonstrates the crucial importance of the nature and the amount of pre-activating reagent over the reactivity.

## CONCLUSION

A systematic study on reactions of **[LFe(CO)$_3$]** with different amounts of $Me_3NO$ were performed to gain a deep understanding on the nature and on the distribution of the iron species formed. The combination of Mössbauer spectroscopy and DFT calculations allows us to evidence the formation of **[LFe(CO)$_2$($NMe_3$)]** and **[LFe(CO)($NMe_3$)$_2$]** upon reaction of $Me_3NO$ on **[LFe(CO)$_3$]**. No trace of the proposed active species, namely [LFe(CO)$_2$], was evidenced neither by Mössbauer spectroscopy nor by $^{13}$C-NMR spectroscopy. When 2 equivalents of oxidant are used, **[LFe(CO)$_2$($NMe_3$)]** is the major iron species formed. This complex may indeed be the key intermediate for the catalysis. We hope this work will provide useful and

valuable information to the scientific community using such type of catalyst to take into account the best activation pathway depending on the targeted transformation. These studies also shed light on the fact that the precatalyst and its corresponding active species exhibit significant differences in their electronic structures and are therefore distinguishable by Mössbauer spectroscopy. It opens the door to Mössbauer investigation of complex catalytic processes involving (cyclopentadienone)iron carbonyl complexes.

## ASSOCIATED CONTENT

**Supporting Information**. The supporting information is available free of charge at https://pubs.acs.org/doi/10.1021/acs.inorgchem.…

Mössbauer spectra and analyses, UV/Vis studies, NMR measurements, computational studies and Cartesian coordinates of computed structures (PDF).

## AUTHOR INFORMATION

### Corresponding Authors

*(Amélie Kochem - Université Grenoble Alpes, CNRS, CEA, LCBM (UMR 5249), F-38000 Grenoble, France; orcid.org/0000-0002-7364-6692; Email: amelie.kochem@cea.fr). *
(Geneviève Blondin - Université Grenoble Alpes, CNRS, CEA, LCBM (UMR 5249), F-38000 Grenoble, France; orcid.org/0000-0002-8045-6328; Email: genevieve.blondin@cea.fr).

### Author Contributions

The manuscript was written through contributions of all authors. All authors have given approval to the final version of the manuscript.

**Notes**

The authors declare no competing financial interest

## ACKNOWLEDGMENTS

Authors acknowledge the Labex ARCANE and CBH-EUR-GS (ANR-17-EURE-0003) for financial support. This work is supported by the French National Research Agency in the framework of the ‘‘Investissements d’avenir’’ program (ANR-15-IDEX-02).

## REFERENCES

(1) Yang, Q.; Wang, Q.; Yu, Z. Substitution of Alcohols by N-Nucleophiles via Transition Metal-Catalyzed Dehydrogenation. *Chem. Soc. Rev.* **2015**, *44* (8), 2305–2329. https://doi.org/10.1039/C4CS00496E.

(2) Shimizu, K. Heterogeneous Catalysis for the Direct Synthesis of Chemicals by Borrowing Hydrogen Methodology. *Catal. Sci. Technol.* **2015**, *5* (3), 1412–1427. https://doi.org/10.1039/C4CY01170H.

(3) Reed-Berendt, B. G.; Polidano, K.; Morrill, L. C. Recent Advances in Homogeneous Borrowing Hydrogen Catalysis Using Earth-Abundant First Row Transition Metals. *Org. Biomol. Chem.* **2019**, *7*, 1595–1607. https://doi.org/10.1039/C8OB01895B.

(4) Quintard, A.; Rodriguez, J. Iron Cyclopentadienone Complexes: Discovery, Properties, and Catalytic Reactivity. *Angew. Chem. Int. Ed.* **2014**, *53* (16), 4044–4055. https://doi.org/10.1002/anie.201310788.

(5) Yan, T.; Feringa, B. L.; Barta, K. Iron Catalysed Direct Alkylation of Amines with Alcohols. *Nat. Commun.* **2014**, *5*, 5602. https://doi.org/10.1038/ncomms6602.

(6) Wei, D.; Darcel, C. Iron Catalysis in Reduction and Hydrometalation Reactions. *Chem. Rev.* **2019**, *119* (4), 2550–2610. https://doi.org/10.1021/acs.chemrev.8b00372.

(7) Irrgang, T.; Kempe, R. 3d-Metal Catalyzed N- and C-Alkylation Reactions via Borrowing Hydrogen or Hydrogen Autotransfer. *Chem. Rev.* **2019**, *119* (4), 2524–2549. https://doi.org/10.1021/acs.chemrev.8b00306.

(8) Pignataro, L.; Gennari, C. Recent Catalytic Applications of (Cyclopentadienone)Iron Complexes. *Eur. J. Org. Chem.* **2020**, *2020* (22), 3192–3205. https://doi.org/10.1002/ejoc.201901925.
(9) Knölker, H.-J.; Heber, J.; Mahler, C. H. Transition Metal-Diene Complexes in Organic Synthesis, Part 14. [1] Regioselective Iron-Mediated [2+2+1] Cycloadditions of Alkynes and Carbon Monoxide: Synthesis of Substituted Cyclopentadienones. *Synlett* **1992**, *1992* (12), 1002–1004. https://doi.org/10.1055/s-1992-21563.
(10) Knölker, H.-J.; Heber, J. Transition Metal-Diene Complexes in Organic Synthesis, Part 18. [1] Iron-Mediated [2+2+1] Cycloadditions of Diynes and Carbon Monoxide: Selective Demetalation Reactions. *Synlett* **1993**, *1993* (12), 924–926. https://doi.org/10.1055/s-1993-22654.
(11) Knölker, H.-J.; Baum, E.; Goesmann, H.; Klauss, R. Demetalation of Tricarbonyl(Cyclopentadienone)Iron Complexes Initiated by a Ligand Exchange Reaction with NaOH—X-Ray Analysis of a Complex with Nearly Square-Planar Coordinated Sodium. *Angew. Chem. Int. Ed.* **1999**, *38* (13–14), 2064–2066. https://doi.org/10.1002/(SICI)1521-3773(19990712)38:13/14<2064::AID-ANIE2064>3.0.CO;2-W.
(12) Carboni, M.; Clémancey, M.; Molton, F.; Pécaut, J.; Lebrun, C.; Dubois, L.; Blondin, G.; Latour, J.-M. Biologically Relevant Heterodinuclear Iron–Manganese Complexes. *Inorg. Chem.* **2012**, *51* (19), 10447–10460. https://doi.org/10.1021/ic301725z.
(13) Charavay, C.; Segard, S.; Edon, F.; Clémancey, M.; Blondin, G. SimuMoss Software, Univ. Grenoble Alpes, CEA/BIG, CNRS, Grenoble, 2012.
(14) Neese, F. The ORCA Program System: The ORCA Program System. *Wiley Interdiscip. Rev. Comput. Mol. Sci.* **2012**, *2* (1), 73–78. https://doi.org/10.1002/wcms.81.
(15) Tao, J.; Perdew, J. P.; Staroverov, V. N.; Scuseria, G. E. Climbing the Density Functional Ladder: Nonempirical Meta–Generalized Gradient Approximation Designed for Molecules and Solids. *Phys. Rev. Lett.* **2003**, *91* (14), 146401. https://doi.org/10.1103/PhysRevLett.91.146401.
(16) Neese, F.; Wennmohs, F.; Hansen, A.; Becker, U. Efficient, Approximate and Parallel Hartree–Fock and Hybrid DFT Calculations. A 'Chain-of-Spheres' Algorithm for the Hartree–Fock Exchange. *Chem. Phys.* **2009**, *356* (1–3), 98–109. https://doi.org/10.1016/j.chemphys.2008.10.036.
(17) Izsák, R.; Neese, F. An Overlap Fitted Chain of Spheres Exchange Method. *J. Chem. Phys.* **2011**, *135* (14), 144105. https://doi.org/10.1063/1.3646921.
(18) van Wüllen, C. Molecular Density Functional Calculations in the Regular Relativistic Approximation: Method, Application to Coinage Metal Diatomics, Hydrides, Fluorides and Chlorides, and Comparison with First-Order Relativistic Calculations. *J. Chem. Phys.* **1998**, *109* (2), 392–399. https://doi.org/10.1063/1.476576.
(19) van Lenthe, E.; Snijders, J. G.; Baerends, E. J. The Zero- order Regular Approximation for Relativistic Effects: The Effect of Spin–orbit Coupling in Closed Shell Molecules. *J. Chem. Phys.* **1996**, *105* (15), 6505–6516. https://doi.org/10.1063/1.472460.
(20) Weigend, F.; Ahlrichs, R. Balanced Basis Sets of Split Valence, Triple Zeta Valence and Quadruple Zeta Valence Quality for H to Rn: Design and Assessment of Accuracy. *Phys. Chem. Chem. Phys.* **2005**, *7* (18), 3297–3305. https://doi.org/10.1039/b508541a.

(21) Pantazis, D. A.; Chen, X.-Y.; Landis, C. R.; Neese, F. All-Electron Scalar Relativistic Basis Sets for Third-Row Transition Metal Atoms. *J. Chem. Theory Comput.* **2008**, *4* (6), 908–919. https://doi.org/10.1021/ct800047t.
(22) Grimme, S.; Antony, J.; Ehrlich, S.; Krieg, H. A Consistent and Accurate *Ab Initio* Parametrization of Density Functional Dispersion Correction (DFT-D) for the 94 Elements H-Pu. *J. Chem. Phys.* **2010**, *132* (15), 154104. https://doi.org/10.1063/1.3382344.
(23) Grimme, S.; Ehrlich, S.; Goerigk, L. Effect of the Damping Function in Dispersion Corrected Density Functional Theory. *J. Comput. Chem.* **2011**, *32* (7), 1456–1465. https://doi.org/10.1002/jcc.21759.
(24) Klamt, A.; Schüürmann, G. COSMO: A New Approach to Dielectric Screening in Solvents with Explicit Expressions for the Screening Energy and Its Gradient. *J Chem Soc Perkin Trans 2* **1993**, (5), 799–805. https://doi.org/10.1039/P29930000799.
(25) Neese, F. Prediction and Interpretation of the 57Fe Isomer Shift in Mössbauer Spectra by Density Functional Theory. *Inorg. Chim. Acta* **2002**, *337*, 181–192. https://doi.org/10.1016/S0020-1693(02)01031-9.
(26) Sinnecker, S.; Slep, L. D.; Bill, E.; Neese, F. Performance of Nonrelativistic and Quasi-Relativistic Hybrid DFT for the Prediction of Electric and Magnetic Hyperfine Parameters in $^{57}$ Fe Mössbauer Spectra. *Inorg. Chem.* **2005**, *44* (7), 2245–2254. https://doi.org/10.1021/ic048609e.
(27) Bjornsson, R.; Neese, F.; DeBeer, S. Revisiting the Mössbauer Isomer Shifts of the FeMoco Cluster of Nitrogenase and the Cofactor Charge. *Inorg. Chem.* **2017**, *56* (3), 1470–1477. https://doi.org/10.1021/acs.inorgchem.6b02540.
(28) Römelt, M.; Ye, S.; Neese, F. Calibration of Modern Density Functional Theory Methods for the Prediction of $^{57}$ Fe Mössbauer Isomer Shifts: Meta-GGA and Double-Hybrid Functionals. *Inorg. Chem.* **2009**, *48* (3), 784–785. https://doi.org/10.1021/ic801535v.
(29) Harris, T. V.; Szilagyi, R. K. Comparative Assessment of the Composition and Charge State of Nitrogenase FeMo-Cofactor. *Inorg. Chem.* **2011**, *50* (11), 4811–4824. https://doi.org/10.1021/ic102446n.
(30) Wolinski, K.; Hinton, J. F.; Pulay, P. Efficient Implementation of the Gauge-Independent Atomic Orbital Method for NMR Chemical Shift Calculations. *J. Am. Chem. Soc.* **1990**, *112* (23), 8251–8260. https://doi.org/10.1021/ja00179a005.
(31) Stoychev, G. L.; Auer, A. A.; Izsák, R.; Neese, F. Self-Consistent Field Calculation of Nuclear Magnetic Resonance Chemical Shielding Constants Using Gauge-Including Atomic Orbitals and Approximate Two-Electron Integrals. *J. Chem. Theory Comput.* **2018**, *14* (2), 619–637. https://doi.org/10.1021/acs.jctc.7b01006.
(32) Neese, F. Software Update: The ORCA Program System, Version 4.0. *WIREs Comput. Mol. Sci.* **2018**, *8* (1). https://doi.org/10.1002/wcms.1327.
(33) Neese, F. A Critical Evaluation of DFT, Including Time-Dependent DFT, Applied to Bioinorganic Chemistry. *J. Biol. Inorg. Chem.* **2006**, *11* (6), 702–711. https://doi.org/10.1007/s00775-006-0138-1.
(34) Pearson, A. J.; Shively, R. J. Iron Carbonyl Promoted Cyclocarbonylation of 3-Hydroxy .Alpha.,.Omega.-Diynes To Give (Cyclopentadienone)Iron Tricarbonyl Complexes. *Organometallics* **1994**, *13* (2), 578–584. https://doi.org/10.1021/om00014a032.
(35) Eekhof, J. H.; Hogeveen, H.; Kellogg, R. M. Intermediate Compound in the Decomplexation of a Tricarbonyl Iron Complex Using Trimethylamine Oxide. *J. Chem. Soc. Chem. Commun.* **1976**, (16), 657. https://doi.org/10.1039/c39760000657.

(36) Plank, T. N.; Drake, J. L.; Kim, D. K.; Funk, T. W. Air-Stable, Nitrile-Ligated (Cyclopentadienone)Iron Dicarbonyl Compounds as Transfer Reduction and Oxidation Catalysts. *Adv. Synth. Catal.* **2012**, *354* (4), 597–601. https://doi.org/10.1002/adsc.201100896.

(37) Casey, C. P.; Guan, H. Cyclopentadienone Iron Alcohol Complexes: Synthesis, Reactivity, and Implications for the Mechanism of Iron-Catalyzed Hydrogenation of Aldehydes. *J. Am. Chem. Soc.* **2009**, *131* (7), 2499–2507. https://doi.org/10.1021/ja808683z.

(38) Pearson, A. J.; Shively, R. J.; Dubbert, R. A. Iron Carbonyl Promoted Conversion of .Alpha.,.Omega.-Diynes to (Cyclopentadienone)Iron Complexes. *Organometallics* **1992**, *11* (12), 4096–4104. https://doi.org/10.1021/om00060a028.

(39) Knölker, H.-J.; Goesmann, H.; Klauss, R. A Novel Method for the Demetalation of Tricarbonyliron-Diene Complexes by a Photolytically Induced Ligand Exchange Reaction with Acetonitrile. *Angew. Chem. Int. Ed.* **1999**, *38* (5), 702–705. https://doi.org/10.1002/(SICI)1521-3773(19990301)38:5<702::AID-ANIE702>3.0.CO;2-W.

(40) Lehnherr, D.; Ji, Y.; Neel, A. J.; Cohen, R. D.; Brunskill, A. P. J.; Yang, J.; Reibarkh, M. Discovery of a Photoinduced Dark Catalytic Cycle Using *in Situ* LED-NMR Spectroscopy. *J. Am. Chem. Soc.* **2018**, *140* (42), 13843–13853. https://doi.org/10.1021/jacs.8b08596.

(41) Pan, H.-J.; Ng, T. W.; Zhao, Y. Iron-Catalyzed Amination of Alcohols Assisted by Lewis Acid. *Chem. Commun.* **2015**, *51* (59), 11907–11910. https://doi.org/10.1039/C5CC03399C.

(42) Zhou, S.; Fleischer, S.; Junge, K.; Beller, M. Cooperative Transition-Metal and Chiral Brønsted Acid Catalysis: Enantioselective Hydrogenation of Imines To Form Amines. *Angew. Chem. Int. Ed.* **2011**, *50* (22), 5120–5124. https://doi.org/10.1002/anie.201100878.

For Table of Contents Only

(cyclopentadienone)iron carbonyl complexes are versatile catalysts for hydrogenation or transfer hydrogenation reactions including the *N*-alkylation of amines with alcohols. In this study, we report on the species formed during the course of the pre-catalyst activation with the $Me_3NO$ chemical reagent.